Decompression during Late Proterozoic Al_2SiO_5 Triple-Point Metamorphism at Cerro Colorado, New Mexico

Katherine R. Barnhart,[1,*] *Pamela J. Walsh,*[2] *Lincoln S. Hollister,*[2] *Christopher G. Daniel,*[3] *and Christopher L. Andronicos*[4]

1. Department of Geological Sciences, University of Colorado, Boulder, Colorado 80309; 2. Department of Geosciences, Princeton University, Princeton, New Jersey 08544; 3. Department of Geology, Bucknell University, Lewisburg, Pennsylvania 17837; 4. Earth and Atmospheric Sciences Department, Purdue University, West Lafayette, Indiana 47907

ABSTRACT

An outstanding problem in understanding the late Proterozoic tectonic assembly of the southwest is identifying the tectonic setting associated with regional metamorphism at 1.4 Ga. Both isobaric heating and cooling, and counterclockwise looping *PT* paths are proposed for this time. We present a study of the Proterozoic metamorphic and deformation history of the Cerro Colorado area, southern Tusas Mountains, New Mexico, which shows that the metamorphism in this area records near-isothermal decompression from 6 to 4 kbar at ca. 1.4 Ga. We do not see evidence for isobaric heating at this time. Decompression from peak pressures is recorded by the reaction Ms + Grt = St + Bt, with a negative slope in *PT* space; the reaction Ms + Grt = Sil + Bt, which is nearly horizontal in *PT* space; and partial to total pseudomorphing of kyanite by sillimanite during the main phase of deformation. The clearest reaction texture indicating decompression near peak metamorphic temperature is the replacement of garnet by clots of sillimanite, which are surrounded by halos of biotite. The sillimanite clots, most without relict garnet in the cores and with highly variable aspect ratios, are aligned. They define a lineation that formed with the dominant foliation. An inverted metamorphic gradient is locally defined by sillimanite-garnet schists (625°C) structurally above staurolite-garnet schists (550°C) and implies ductile thrusting during the main phase of deformation. The exhumation that led to the recorded decompression was likely in response to crustal thickening due to ductile thrusting and subsequent denudation.

Online enhancements: appendix tables.

Introduction

An unresolved problem for understanding the Proterozoic tectonic assembly of the southwestern United States is identifying the shape of the *PT* path—and thus the tectonic setting—associated with regional metamorphism at 1.4 Ga. This metamorphic event is characterized by regional temperatures of 500°–600°C recorded at relatively shallow depths (10–12 km), corresponding to 3.5–4.0 kbar (Grambling 1988; Williams 1991; Shaw et al. 2005). It produced world-renowned triple-point mineral assemblages that include andalusite, kyanite, and sillimanite at pressures and temperatures close to those of the Al_2SiO_5 invariant point (Holdaway 1978; Grambling 1981). The triple-point mineral assemblages have been argued to result from isobaric heating and cooling (Grambling 1988), cooling during decompression (Grambling et al. 1989; Grambling and Dallmeyer 1993), and polymetamorphic clockwise looping *PT* paths that reflect several episodes of metamorphism separated by large periods of time (Williams and Karlstrom 1996; Pedrick et al. 1998).

In northern New Mexico, southern Colorado, and Arizona, two major orogenic events are widely recognized (e.g., Bowring and Karlstrom 1990). The earliest involved the accretion of juvenile crust of the Yavapai/Colorado Province to the Archean Wyoming Province across the Cheyenne belt (Karlstrom and Houston 1984). The nature of the juve-

Manuscript received June 14, 2011; accepted March 5, 2012.
* Author for correspondence; e-mail: barnhark@colorado.edu.

[The Journal of Geology, 2012, volume 120, p. 385–404] 0022-1376/2012/12004-0003$15.00. DOI: 10.1086/665793

nile crust is controversial; suggested mechanisms of formation include accreted arcs (Karlstrom and Bowring 1988; Tyson et al. 2002), reworked oceanic crust (Cavosie and Selverstone 2003), and extended and recycled continental crust of the Trans-Hudson orogen (Hill and Bickford 2001; Bickford and Hill 2007). Between 1.7 and 1.6 Ga, the Mazatzal Province of Arizona and New Mexico was accreted to the southern margin of the Yavapai Province; this produced a broad transition zone between the two provinces (Shaw and Karlstrom 1999). The Tusas Mountains, including Cerro Colorado, lie within this transition zone.

Complicating the above tectonic history are widespread and voluminous plutons with ages that range from 1.46 to 1.35 Ga, the so-called 1.4-Ga anorogenic plutonic suite (Anderson 1983). Although evidence exists that the plutons were emplaced in a compressive or transpressive strain field (e.g., Nyman et al. 1994; Kirby et al. 1995; Ferguson et al. 2004), the exact tectonic environment into which the plutons were emplaced remains debated. Evidence for regional metamorphism during the 1.4-Ga plutonic events comes from biotite, hornblende, and muscovite Ar cooling dates determined from rocks throughout northern New Mexico and southern Colorado (Grambling and Dallmeyer 1993; Karlstrom et al. 1997; Shaw et al. 2005). This is a particularly important data set, since it shows that the triple-point metamorphic terrane cooled from peak metamorphic temperatures after 1.4 Ga. Because no older Ar dates have been determined from within sillimanite grade rocks, either prograde metamorphism occurred at this time (Grambling and Dallmeyer 1993) or the region was reheated and remained hot long enough to completely reset the Ar isotopic systematics (Shaw et al. 2005).

In a study of metamorphic reaction textures coupled with monazite geochronology in the Picuris Mountains of northern New Mexico, Daniel and Pyle (2006) argued that amphibolite facies metamorphism followed a clockwise *PT* loop at temperatures slightly above the Al_2SiO_5 triple point and included a nearly isobaric drop in pressure from 5 to 4 kbar. Ion probe monazite dates presented by Daniel and Pyle (2006) are consistent with an interpretation that all metamorphism and deformation occurred between 1.43 and 1.39 Ga. Palinspastic restorations of post-Precambrian deformation (Karlstrom and Daniel 1993; Cather et al. 2006) show that the southern Tusas and Picuris Mountains (fig. 1) were adjacent and contiguous at 1.4 Ga. Detrital U-Pb zircon dates on synorogenic successions in the Picuris require deposition and associated regional metamorphism after 1453 Ma

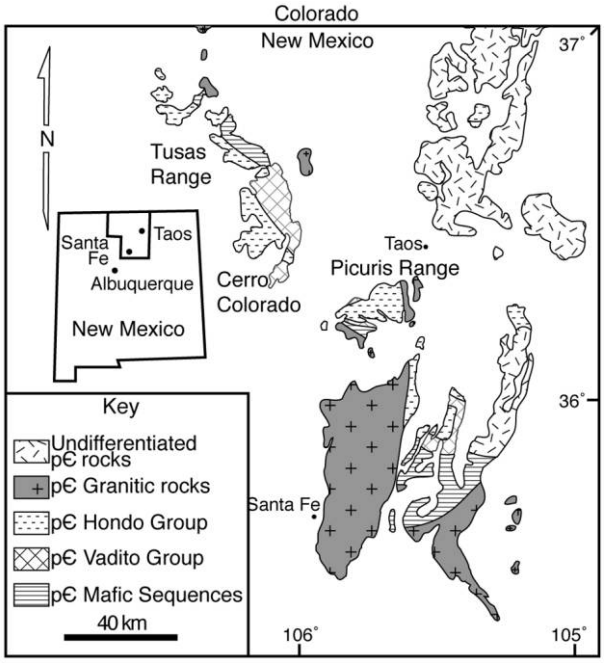

Figure 1. Geologic map of Precambrian rocks of northern New Mexico showing the location of Cerro Colorado within the Tusas Range. Redrawn from figure 1 of Williams (1991).

(Jones et al. 2011). These observations support the interpretation that regional amphibolite facies metamorphism in the Tusas Mountains occurred at ca. 1.4 Ga and not earlier.

The rocks at Cerro Colorado (fig. 2) are among the highest grade of the triple-point rocks (Grambling et al. 1989). The Tusas Mountains as a whole represent a tilted upper crustal section, with low-grade metamorphic rocks exposed in the northern part of the range and sillimanite grade rocks occurring in the southern Tusas Mountains, at Cerro Colorado (fig. 1; Williams 1991). The metamorphic grade in the range increases from ~420°C and 3 kbar in the northwest portion of the range to ~600°C and 5 kbar in the southeast (Grambling et al. 1989).

In this article, we demonstrate that metamorphic rocks from Cerro Colorado in the southern Tusas Mountains of northern New Mexico (fig. 1) provide insight on the *PT* path followed by this high *T*/low *P* metamorphic terrane. On the basis of our observations of mineral reaction texture, mineral zoning, *PT* estimates, and structure, we conclude that the Cerro Colorado area decompressed from 6 to 4 kbar during a phase of ductile thrusting at or near peak metamorphic temperatures of about 600°C. The decompression is recorded by reactions involving Fe-Mg silicates. Decompression is inferred to have oc-

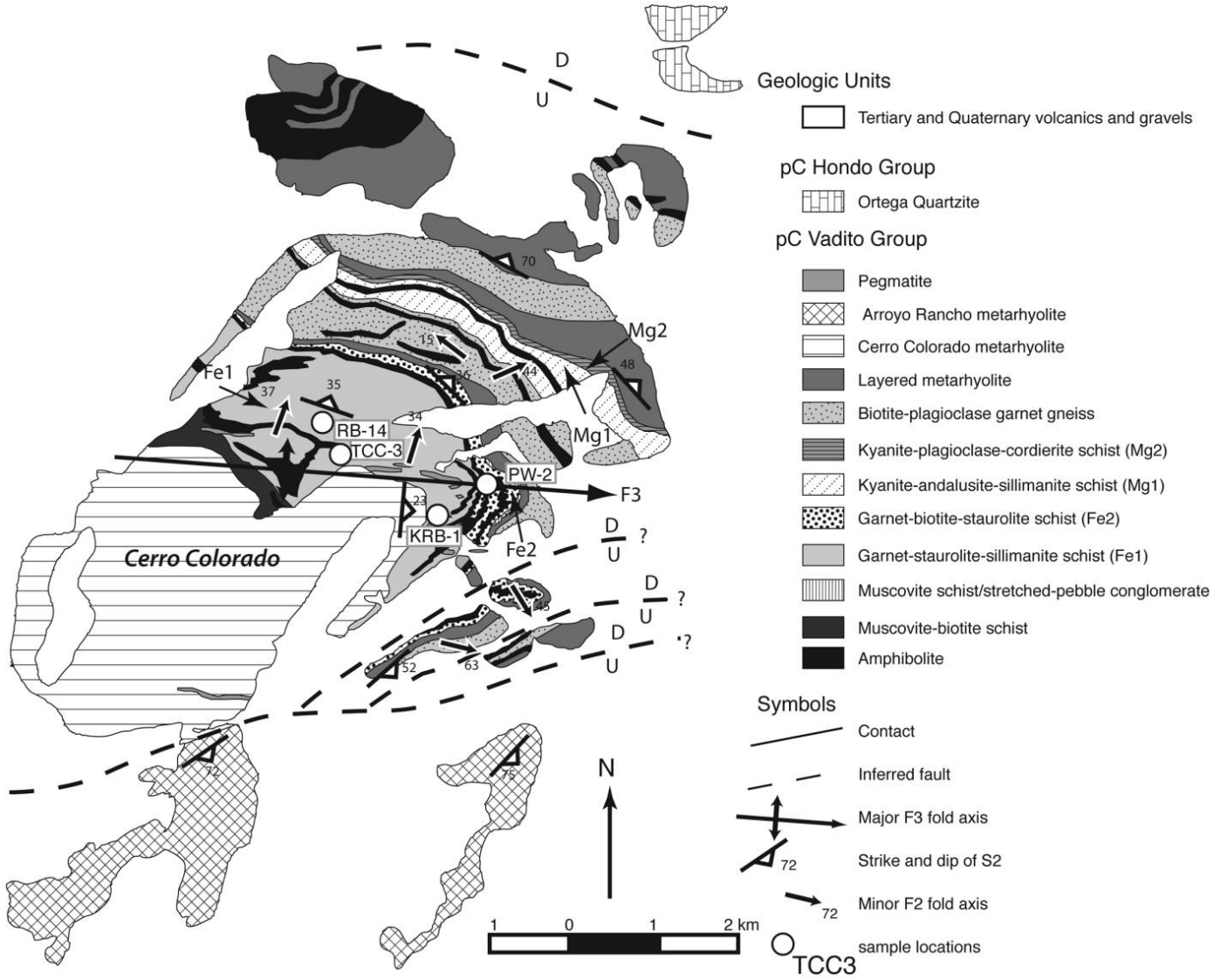

Figure 2. Geologic map of Cerro Colorado from Bishop (1997). Shows location of map-scale F_3 fold, measurements of S_2, mapped extent of major lithologies, locations of the staurolite schists (samples TCC-3 and RB-14), and locations of the garnet-sillimanite schists (samples KRB-1 and PW-2).

curred at about 1.4 Ga, on the basis of deformation and reaction textures coupled with timing constraints provided by reported cooling and metamorphic mineral dates for the region. The observed decompression, together with our interpretations of garnet zoning patterns, is not consistent with models of isobaric reheating at 3–4 kbar from a steady state geothermal gradient previously proposed for this area (e.g., Williams and Karlstrom 1996, their fig. 2; Karlstrom et al. 2004, their fig. 13). The observed decompression is consistent with observations from the nearby Picuris (Daniel and Pyle 2006; Jones et al. 2011). Our results in general support the clockwise *PT* loops described for several regions of northern New Mexico (Williams 1991; Grambling and Dallmeyer 1993; Daniel and Pyle 2006). However, our observations of the decompression reactions among Fe-Mg silicates coupled with microstructural observations and garnet zoning patterns imply that the decompression phase of the loops occurred at about 1.4 Ga rather than at 1.7–1.6 Ga. Our conclusions are consistent with those of Daniel and Pyle (2006) for the nearby Picuris Mountains (fig. 1) and require reevaluation of current tectonic models for Proterozoic orogeny in northern New Mexico.

Geologic Setting of Cerro Colorado, Southern Tusas Mountains

The Cerro Colorado area is located in the southern Tusas Mountains (fig. 1). The Tusas Mountains define the western margin of the Rio Grande Rift and its transition to the Colorado Plateau to the west. They are the southern extension of the San Juan Mountains of southern Colorado. The Proterozoic geologic history of the area is given by Williams (1991), Williams et al. (1999*a*), and Koning et al. (2005). According to Grambling et al. (1989), *PT* conditions in the Tusas Mountains increased from 420°C and 3 kbar in the northwest to about 600°C and 5 kbar in the southeast.

A metarhyolite forms the peak, Cerro Colorado (fig. 2), from which the area takes its name. This metarhyolite is part of the 1.7-Ga Vadito Group and was interpreted by Treiman (1977) to be a shallow intrusive body. It has a reported age of ca. 1.7 Ga (Bishop 1997). No 1.4-Ga plutons are exposed in the Cerro Colorado area, but coarse pegmatites crosscut the dominant foliation. The pegmatites form sills oriented roughly parallel to S_3 and have S_3 developed in their margins (Williams et al. 1999*a*). Monazite, titanite, and xenotime from these pegmatites yielded U-Pb dates of 1.41–1.42 Ga (Williams et al. 1999*a*). The locations of pegmatites are marked in figure 2; they are likely syn- or post-D_3 in age and place a younger limit on the timing of D_2 deformation. There are also reports (Bishop 1997; Williams et al. 1999*a*, 1999*b*) of monazite domains included in the syntectonic, peak metamorphic staurolite porphyroblasts that yield in situ electron microprobe U–Th–total Pb dates ranging from 1.4 to 1.47 Ga (Williams et al. 1999*a*, 1999*b*). Aligned inclusions within this monazite domain indicate that at least one deformational event occurred before the metamorphism at 1.4–1.45 Ga (Williams et al. 1999*b*). Lanzirotti et al. (1996) report $^{207}Pb/^{235}U$ dates on monazite separates from around a quartzite vein of 1443 Ma from the Tusas Mountains and U-Pb monazite dates on elongate monazite aligned in staurolite of 1472 ± 8 Ma. The published and unpublished dates from the Cerro Colorado area suggest that the metamorphism occurred at ca. 1.4 Ga.

Treiman (1977) and Bishop (1997) mapped compositionally distinct porphyroblast-bearing layers (fig. 2) in the Cerro Colorado area. These include garnet-staurolite-sillimanite schist, garnet-biotite-staurolite schist, kyanite-sillimanite schist, andalusite schist, and cordierite-sillimanite schist. Bishop (1997) showed that the layers containing garnet and staurolite have distinctly higher Fe/Mg than those containing cordierite. In this article, we consider only metamorphic assemblages in the Fe rich units, and we focus on four samples (fig. 2) that record the high-temperature decompression.

Bishop (1997) argued that the ca. 1.4-Ga metamorphism was in response to isobaric heating. Her main evidence for this conclusion is the late sillimanite together with thermobarometry, indicating pressures of 3–4 kbar. In this article, we show that the compositions of the minerals reequilibrated at 3–4 kbar from higher pressure and that the sillimanite growth was primarily in response to reactions that occurred during decompression.

The deformational history of the Proterozoic rocks of northern New Mexico includes at least three major fabric-forming events defined by overprinting relationships (Williams et al. 1999*a*). In this article, we follow the classification scheme of Williams et al. (1999*a*) in referring to deformation events (D), associated folding (F) and foliation (S) development, and metamorphic events (M). In the Cerro Colorado region, the first deformational event manifests as an early bedding-parallel foliation (S_1); the second as the dominant foliation (S_2); and the third in upright, east-striking folds (F_3) with a variably developed foliation (S_3; Williams et al.

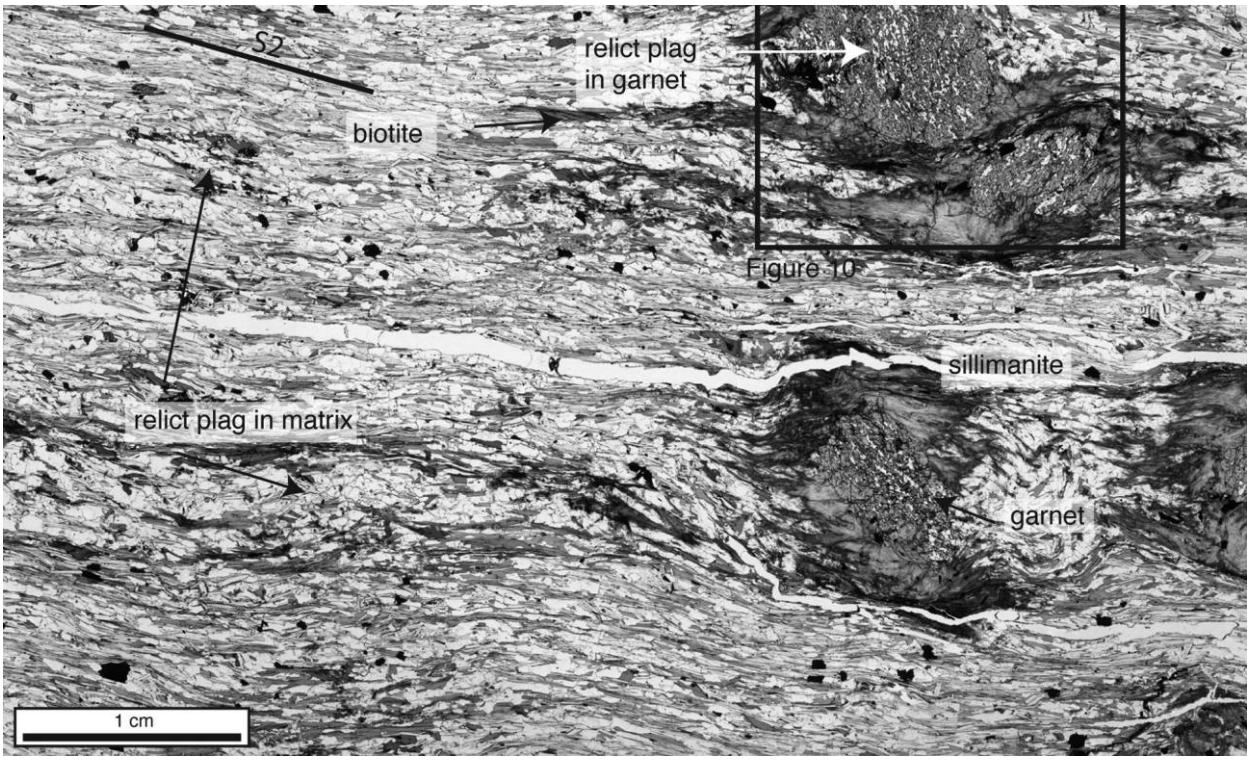

Figure 3. Photomicrograph of sample KRB-1. The dominant foliation is S_2. Garnet is overgrown by sillimanite and biotite. Plagioclase is present in the matrix and is included in one garnet. A staurolite fragment is present in the matrix. Inset shows location of the X-ray area scan of figure 10. Thin section is cut perpendicular to foliation and parallel to lineation. A color version of this figure is available in the online edition or from the *Journal of Geology* office.

1999*a*). In the Cerro Colorado area, the dominant map-scale structure is a kilometer-scale F_3 fold (fig. 2; Treiman 1977; Bishop 1997).

Petrologic and Field Microstructural Observations

Reaction Textures. We first describe the metamorphic reactions preserved in the Fe-rich rocks of the Cerro Colorado area that record decompression. We follow the mineral abbreviation conventions of Whitney and Evans (2010).

Sample KRB-1 (table A1 [tables A1–A7 are available in the online edition or from the *Journal of Geology* office]) preserves a reaction texture in which partially resorbed garnets are surrounded by mats of sillimanite (fig. 3). Biotite is abundant around the sillimanite mats, and muscovite and biotite occur in the matrix. The implied reaction is

$$\text{Ms} + \text{Grt} = \text{Sil} + \text{Bt}. \quad (1)$$

In sample TCC-3 (table A1; fig. 4), muscovite is absent. Garnet is partially resorbed, and concentrations of sillimanite occur in embayments in the garnet. Staurolite is fractured, and biotite occurs between the fragments. Sillimanite also occurs in embayments in the staurolite. The texture is evidence for the reaction

$$\text{Ms} + \text{Grt} + \text{St} = \text{Sil} + \text{Bt}, \quad (2)$$

which progressed until the muscovite was removed from the assemblage. We note that this reaction did not progress as far as the reaction observed in sample KRB-1 because of the removal of muscovite. This is why many of the garnets retain unembayed crystal faces.

In sample RB-14, staurolite clearly grew over garnet (fig. 5) and therefore postdates early garnet. Foliation in the garnet merges at the rims with the planar foliation (S_2) of the matrix, and staurolite grew over this planar foliation as well as over the garnet.

The reaction recorded in sample RB-14 is

$$\text{Ms} + \text{Grt} = \text{St} + \text{Bt}. \quad (3)$$

In sample PW-2 (table A1), small euhedral garnets are distributed throughout the sample and are present both in the matrix and within sillimanite clots

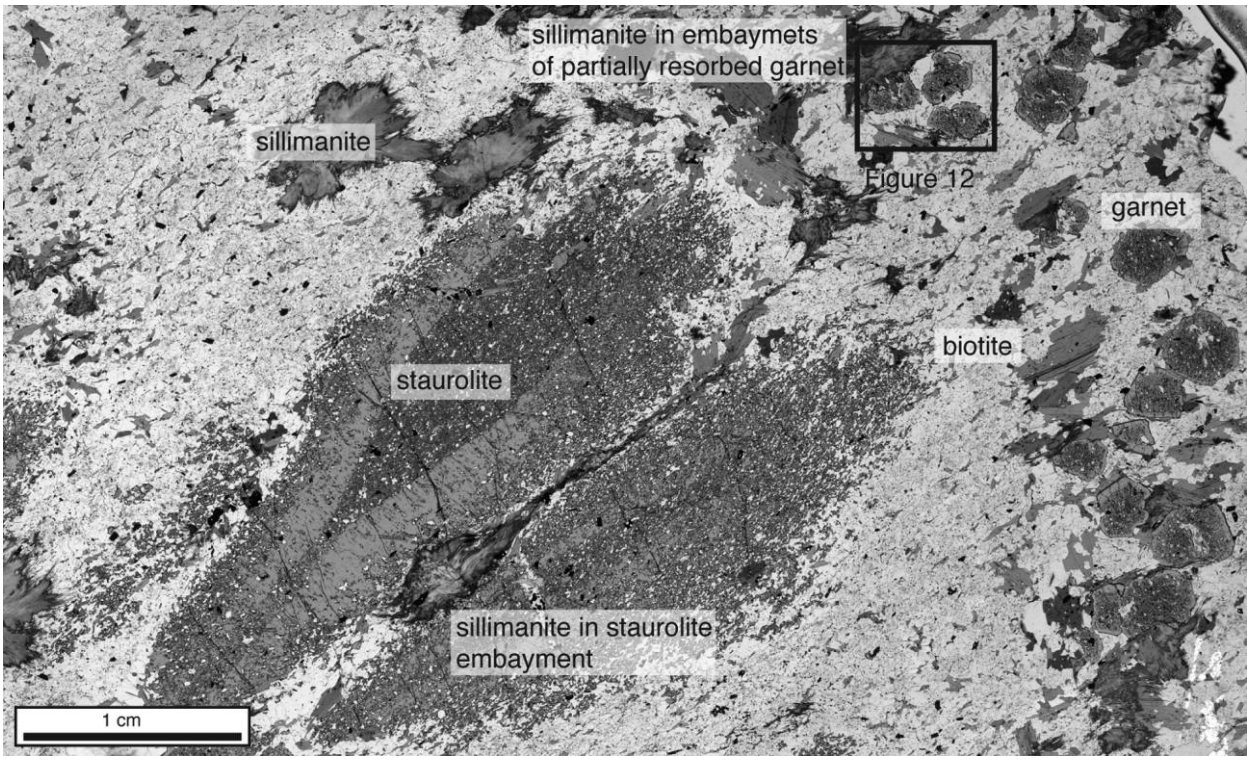

Figure 4. Photomicrograph of sample TCC-3 cut perpendicular to foliation and parallel to lineation. Sillimanite is found in embayments in garnet and staurolite. No muscovite is present. Inset shows location of X-ray area scan of figure 12. A color version of this figure is available in the online edition or from the *Journal of Geology* office.

(fig. 6). Rocks containing sillimanite clots without included garnet remnants are common in the Cerro Colorado area (Bishop 1997), and many of these contain garnets similar to those that occur in PW-2.

In samples KRB-1 and TCC-3, resorption of garnet continued until either all remaining garnet fragments were armored within sillimanite mats (KRB-1) or muscovite was totally consumed by reaction, as in sample TCC-3, discussed above.

Fragments of staurolite in sample KRB-1 (fig. 7) and in the unit from which sample KRB-1 was collected, as well as the abundance of staurolite in the other two samples, imply that temperatures were above the staurolite-out reactions for the sillimanite schists (KRB-1, PW-2) but were below those reactions for the staurolite schists (TCC-3, RB-14).

The contrast of textures from samples KRB-1 and PW-2 imply two phases of garnet growth. In sample KRB-1, garnet was in the rock before reaction 1 and was partially resorbed by the reaction. We interpret the sillimanite clots in sample PW-2 as an indication that the earlier generation of garnet preserved in samples KRB-1 and TCC-3 was present but completely reacted out. The small garnets located both in the matrix and within the sillimanite mats suggest a second phase of growth of garnet at *PT* conditions within the stability field of sillimanite.

Field Microstructure. The relation of the microstructures (foliation, lineation) to mineral growth defines the sequence of growth of the porphyroblasts and constrains the *PT* paths recorded by the above reactions. According to Williams (1991) and Bishop (1997), deformation in the area began with north-directed thrusting and the development of the dominant schistosity (S_2; fig. 2). S_2 contains intrafolial recumbent isoclines of a schistosity interpreted by Williams (1991) to have formed during D_1.

The first generation of garnet grew over crenulations that are preserved as inclusion trails in the garnets. These crenulations could be preserved from an earlier (S_1) foliation or be an early phase of S_2, as described by Williams et al. (1999*a*). In any case, these inclusion trails asymptotically merge at the garnet borders with the S_2 foliation, which indicates garnet growth during D_2. Garnet included in staurolite has inclusion trails from the early crenulations, but staurolite in the samples we studied has only straight inclusion trails that are par-

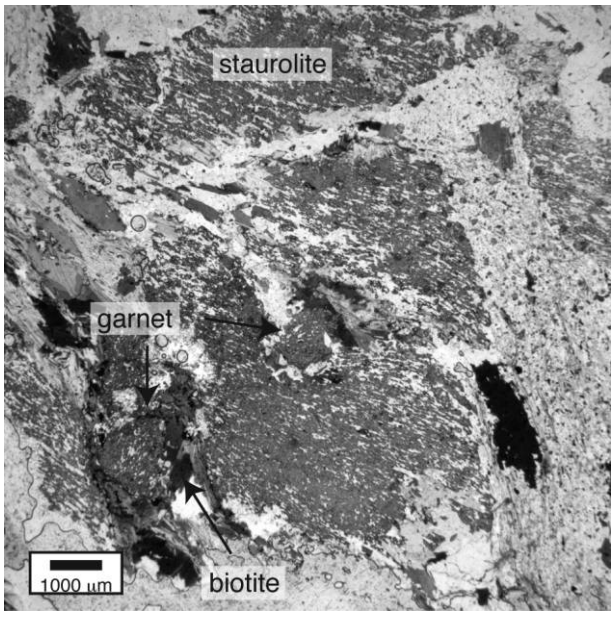

Figure 5. Photomicrograph of sample RB-14 cut perpendicular to foliation and parallel to lineation. Garnet is overgrown by staurolite. Biotite and sillimanite occur adjacent to the garnets. The foliation in the garnet merges at grain rims into the main matrix foliation; staurolite overgrows this foliation. A color version of this figure is available in the online edition or from the *Journal of Geology* office.

allel with the main foliation (S_2), indicating that staurolite growth was after garnet growth and during or after D_2.

Although the aspect ratios of the clots of sillimanite in the sillimanite-rich schists vary from place to place, the long axis of the clots defines the L_2 lineation within the S_2 foliation (figs. 3, 8). The short axis of the clots is perpendicular to S_2. Within the clots, the individual sillimanite needles vary in orientation, including being perpendicular to S_2, but the majority of the sillimanite needles lie parallel to S_2. In figure 8, poles to the dominant foliation (S_2) define a great circle with a π axis of 21° to 086°. Because this orientation is parallel to the F_3 fold hinges, we interpret the microstructural observations to indicate that F_3 folded S_2.

Lineation orientations are scattered along the great circle defined by the poles to S_2 (fig. 8). The measured lineations are defined by the elongation direction of clots of sillimanite. We interpret the geometry of the sillimanite clots to indicate that the clots formed during D_2 and before D_3. This is confirmed by field observations of elongate sillimanite clots crenulated by F_3. Field and petrographic observations suggest that some sillimanite also grew during F_3. We conclude that the conditions of formation of S_2 and of F_3 structures were within the sillimanite stability field. Our observations are consistent with those of Treiman (1977), Williams (1991), and Bishop (1997).

Bent kyanite occurs in isoclinally folded quartz veins in the high Fe/Mg sequence (fig. 9); these folded veins have axial planes parallel to S_2. Kyanite that grew in S_2 extension gashes in a quartz vein are aligned across the vein in the L_2 direction. Sillimanite partially to completely pseudomorphs the earlier kyanite. Accordingly, the *PT* paths of the Fe/Mg layers of Cerro Colorado began in the kyanite stability field and passed into the sillimanite stability field.

Mineral Compositions

In order to better constrain the *PT* conditions experienced by the samples, we acquired qualitative X-ray area scans and quantitative points and transects of silicate mineral compositions for each sample. Here we first present the analytical methods, followed by descriptions of the zoning profiles.

Analytical Methods. The samples were analyzed on the University of Massachusetts Cameca SX-50 microprobe equipped with four spectrometers. The microprobe was calibrated on natural and synthetic standards. All qualitative X-ray area maps and quantitative point measurements and line scans were taken with a fixed beam, with the stage moving automatically under the 1-μm diameter beam. The analysis procedure is described by Barnhart (2008).

X-ray area maps were made of four elements—Ca, Mg, Mn, and K—in order to capture zoning in both garnet and plagioclase. No X-ray area maps were made for Fe, since the microprobe had four spectrometers and Fe zonation is likely in the opposite sense of Mg. Point and line analyses measured a variety of elements, depending on the expected chemistry of each mineral.

Representative quantitative analyses for garnet and plagioclase (tables A2, A3) were selected from line scans based on the observed zoning patterns. The compositions of biotite, muscovite, and staurolite (tables A4, A6) were based on point analyses. Biotite analysis points were selected on the basis of weight percent totals and weight percents of K_2O and of FeO + MgO. Plots of total weight percent versus FeO + MgO and of K_2O versus FeO + MgO were made, and the point yielding the greatest of all three is given in table A4. The uncertainty on major elements for a typical microprobe measure-

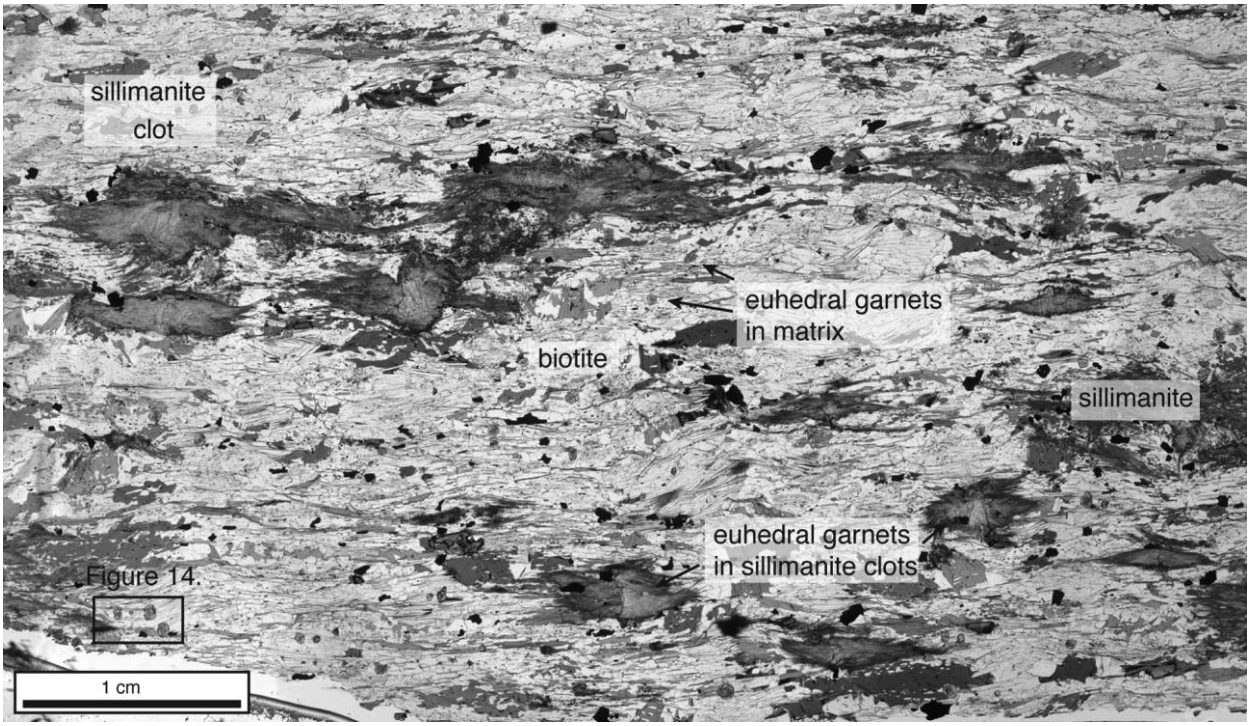

Figure 6. Photomicrograph of sample PW-2 cut perpendicular to foliation and parallel to lineation. Euhedral garnets are present within sillimanite clots in the matrix. Inset outlines area covered by X-ray area scans of figure 14. A color version of this figure is available in the online edition or from the *Journal of Geology* office.

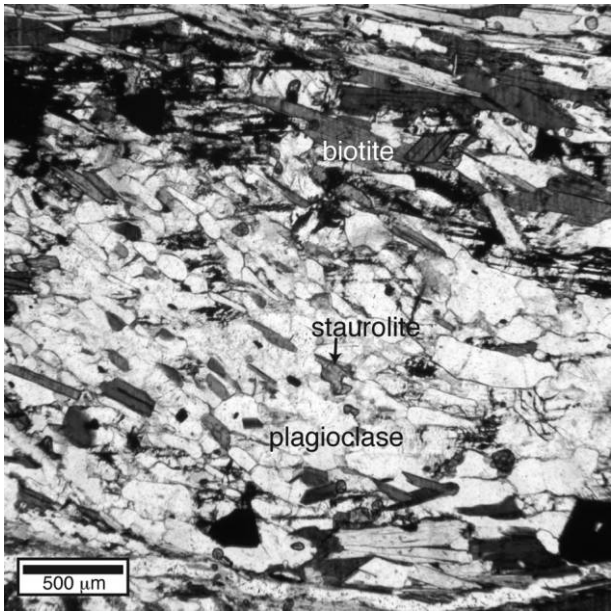

Figure 7. Photomicrograph of staurolite fragments in KRB-1. Muscovite and quartz are also in field of view. A color version of this figure is available in the online edition or from the *Journal of Geology* office.

ment is 1% of the weight percent measured. Propagating that through the formula recalculation for the maximum weight percents measured for MgO, CaO, MnO, and FeO yields maximum uncertainty, in end member molecular components, of ± 0.14 for pyrope, ± 0.07 for grossular, ± 0.27 for spessartine, and ± 0.73 for almandine.

Although the interior of most of the garnet grains is essentially unzoned on the basis of both X-ray area scans and quantitative transects, pronounced compositional zoning is observed near the rims in all analyzed grains. At the garnet rims, cation proportions, especially Mg (and Fe in the opposite sense), change rapidly with respect to distance as the rims are approached. It is thus difficult to determine true "edge" compositions of garnet. The "core" garnet compositions were taken from the interior of the grain where zoning is minimal. The points used for *PT* estimation are labeled on the quantitative line scans of garnet and plagioclase.

The high-resolution, qualitative X-ray area scans presented below illustrate the intricacies of compositional variation in the garnet and the plagioclase. The X-ray scans indicate the relative intensity of a particular spectral line (e.g., Fe Kα) and informed the choice for locations of the quantitative line scans.

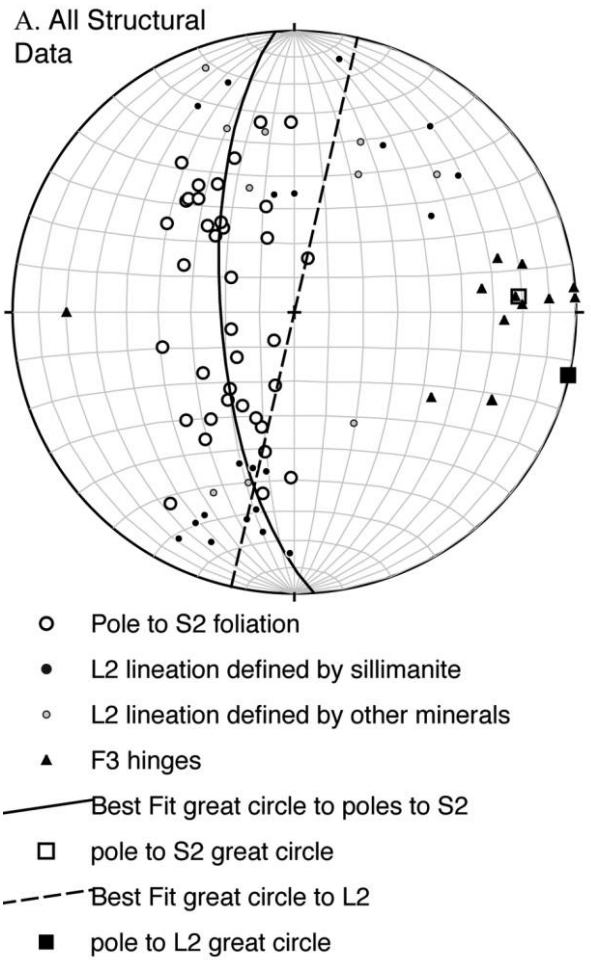

Figure 8. *A*, Stereonet showing foliations, lineations, and fold hinges measured within the high Fe/Mg units of figure 2. S_2 foliation is clearly folded by F_3 folds. L_2 lineation defined by sillimanite and other minerals shows a bimodal distribution. *B*, Outcrop scale observations show elongate sillimanite clots crenulated by F_3. A color version of this figure is available in the online edition or from the *Journal of Geology* office.

In the description of X-ray area scans, we refer to changes in the relative intensity of the observed element. When discussing quantitative line scans, we refer to the changes in the molecular proportion of end member minerals: for garnet, the Ca end member is grossular (Grs), the Fe end member is almandine (Alm), the Mg end member is pyrope (Pyr), and the Mn end member is spessartine (Sps); for plagioclase, the Ca end member is anorthite (An), and the Na end member is albite (Ab). For example, a garnet with Alm 77 has 77% of its octahedral sites occupied by Fe atoms. The X-ray area and line scans demonstrate the response of the garnet and plagioclase compositions to the *PT* path of the rocks. In many of the X-ray area scans, the zoning is subtle; some zoning patterns are difficult to distinguish in the X-ray area maps but are apparent in the quantitative line scans.

Descriptions of X-Ray Area Scans and Quantitative Line Scans. Figure 10 shows X-ray area scans of two garnets from sample KRB-1. Mg decreases sharply within the rims toward all the edges. Notable is the fact that compositional variation at the rim, with Mg sharply dropping toward the edge, delicately follows the outlines of the garnet fragments, although the garnet is an anhedral relict within a sillimanite clot. Mn, on the other hand, decreases slightly at the very edges.

In contrast to the Mg zoning patterns, compositional variation of Ca is not systematic with respect to grain margins. Discrete areas of relatively high grossular are present in the three garnets scanned from sample KRB-1 (fig. 10*B*). Areas of relatively high Ca in the garnet are not correlated with

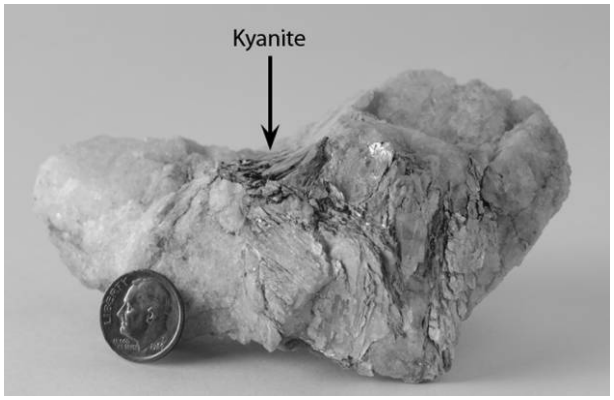

Figure 9. Kyanite in quartz vein. The kyanite is folded around an F_2 fold in the quartz vein. The kyanite is partly replaced by sillimanite and muscovite. A color version of this figure is available in the online edition or from the *Journal of Geology* office.

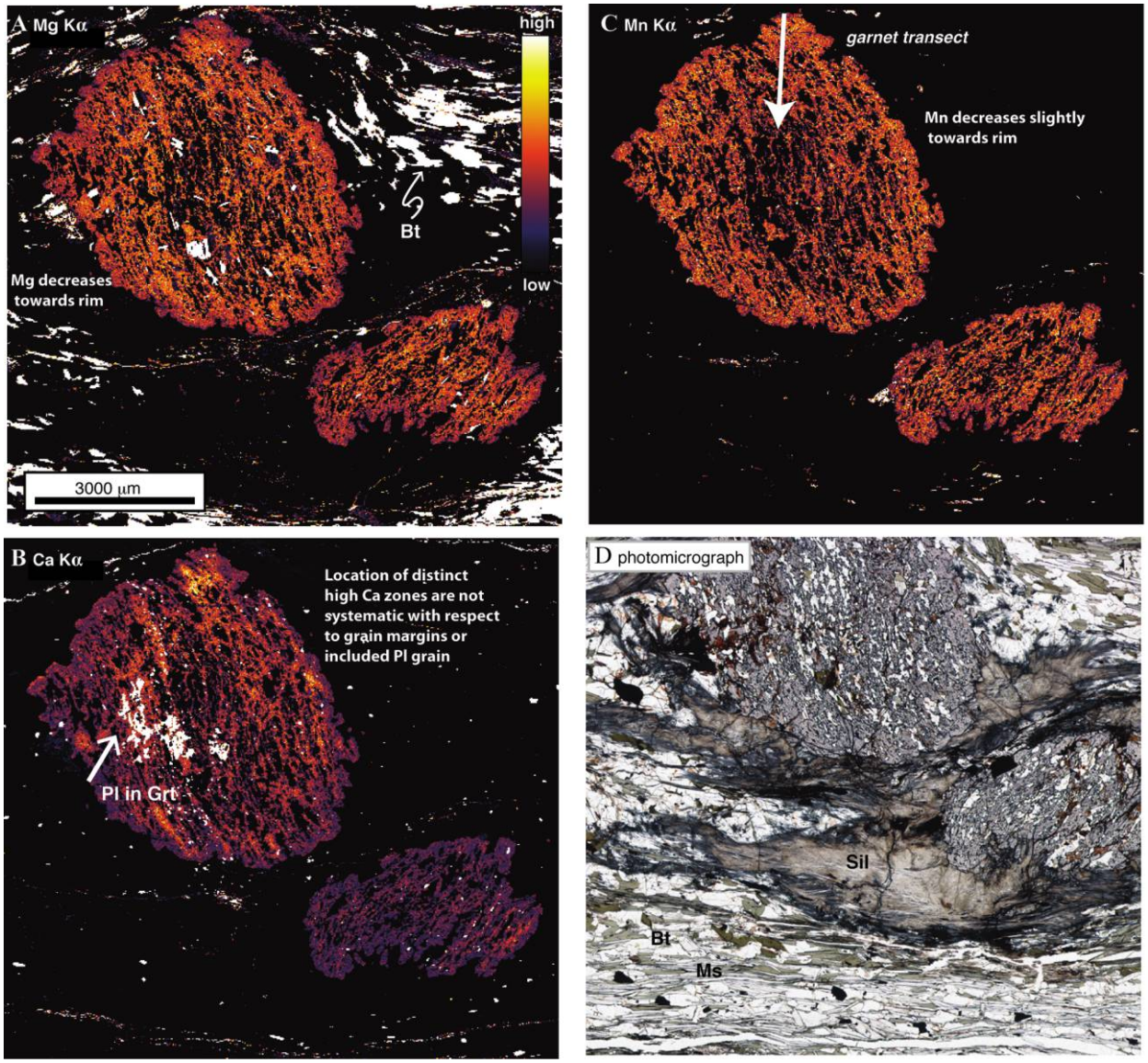

Figure 10. X-ray area scans showing the relative intensity of Mg, Mn, and Ca in the area of sample KRB-1 marked in figure 3. Arrow in *C* shows the location of the quantitative traverse of figure 11. Note the very irregular plagioclase inclusion in *B*. *D* is a photomicrograph of the region of the thin section containing the X-ray scans.

the location of the highly irregular inclusion of plagioclase imaged in figure 10*B*.

Figure 11 shows the zoning profile across a portion of a garnet in sample KRB-1 (location marked in fig. 10*C*). Beginning from the interior of the garnet, the composition is nearly uniform at Alm 73–74, Pyr 6, Grs 6, and Sps 13 until about 200 μm from the edge, where Alm climbs to 77, Pyr and Grs each decrease to 5, and Sps decreases to 12.

A plagioclase within the garnet of sample KRB-1 (the bright grain in fig. 10*B*) has a composition of about An 40.5 except for two points at the edges, which have compositions of about An 36. The plagioclase in the matrix of this sample (fig. 3) has an average composition of An 35.

Garnet in sample TCC-3 (fig. 12) are anhedral and inclusion rich, except for inclusion-free but discontinuous borders. Mg decreases toward the outermost edges. The inclusion-free borders appear to be a relict of garnet that has been partially resorbed.

Figure 13 shows zoning profiles across a garnet in sample TCC-3 from an edge where the garnet appears to have been partially resorbed to the edge of the inclusion-free border. Fe and Mn increase across rims about 100 μm wide toward both edges, and Mg decreases. Grossular is at a plateau value

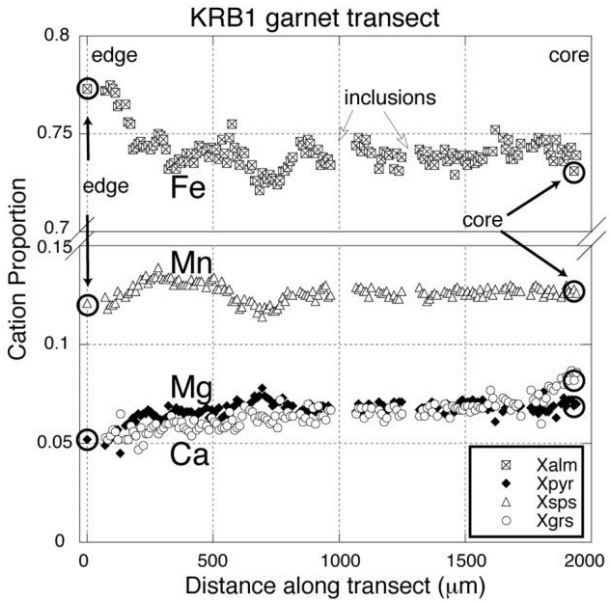

Figure 11. Quantitative transect across garnet in sample KRB-1 along the transect marked in figure 10*C*. The edge and core compositions are given in table A2 (available in the online edition or from the *Journal of Geology* office).

of about 5.8 across most of the garnet, increases in the central portion of the inclusion-free borders, but drops slightly to a rim value of 5.6 at the edge of the inclusion-free border.

Figure 14 shows scans of garnet and matrix in sample PW-2. Garnet is subhedral to euhedral. Mg and Mn are lower—and Fe higher—at the rim than in the cores, and Ca has a relatively low composition trough that is traced around the garnets, close to the rim.

Figure 15 shows zoning profiles across a garnet in PW-2. From a plateau in the core of Alm 58, Fe increases across a 100-μm rim to Alm 60 at the edge. The shape of the Mg profile is similar but with opposite sense, from Pyr 11.5 in the core to Pyr 10 at the edge. Mn increases toward the edges from Sps 27.5 at a plateau to 27.8 about 30 μm from the edge before dropping to 26.2 at the edge. Grossular is 3.1 in the plateau, drops to 2.7 about 30 μm from the edge, and then increases to 3.6 at the rim. In the X-ray area scan (fig. 14), the trough of low Ca in the garnets is continuous around the garnets.

Zoning profiles in plagioclase in PW-2 and TCC-3 are given in figures 16 and 17, respectively. Plagioclase of sample PW-2 has zones of higher Ca (An 25.5) in the center, decreasing to An 20–21 at the rims. Sample TCC-3 has the opposite sense of zoning, with An increasing from An 50 in the core to An 55–60 in the rim, but the zoning is less regular than that in PW-2. The few grains of plagioclase in sample KRB-1 do not show a systematic zoning pattern.

PT Estimates

On the basis of observed mineral assemblages, preserved reaction textures, and measured mineral compositions and zoning patterns, we describe the *PT* paths for staurolite-bearing and sillimanite-bearing assemblages. We used four methods to estimate the *PT* conditions experienced by these samples: development of a petrogenic grid (after Davidson et al. 1997), peak *PT* estimates using TWQ (Berman 1991; http://gsc.nrcan.gc.ca/sw/twq_e.php), compositional zoning patterns of garnet, and a pseudosection calculation using Theriak-Domino (de Capitani and Petrakakis 2010). The petrogenetic grid and zoning patterns constrain the *PT* paths that the samples followed; the TWQ thermobarometry yielded *PT* estimates in the andalusite stability field rather than the sillimanite stability field. Pseudosection analyses using the grossular and anorthite isopleths for sample KRB-1 yielded a *PT* estimate of 4 ± 0.3 kbar and $590° \pm 10°$C for the end of the sillimanite-producing metamorphism (M_2 metamorphism during D_2 deformation).

We note that an issue in comparing the *PT* estimates made by the three different methods is that each method uses a different thermodynamic data set. As such, we do not expect precise concordance of results using the different data sets. However, if the mineral compositions were set during the peak metamorphic conditions, we would expect that the *PT* estimates using different methods and different databases would overlap or at least be close in *PT* space (e.g., Amato et al. 2011). However, *PT* estimates based on the garnet compositions in Fe, Mg, and Mn are inconsistent with the observed mineral assemblages or those predicted by pseudosection analysis. We therefore conclude that the garnet compositions do not record the peak metamorphic equilibrium conditions.

Petrogenetic Grid. The grid of figure 18 serves to illustrate the reactions observed in the high Fe/Mg unit of Cerro Colorado. It has four reactions: (1) Ms + Grt = Sil + Bt, (2) Qz + St = Sil + Grt, (3) Ms + Grt = St + Bt, and (4) Ms + St = Sil + Bt. Reaction 1 is slightly positive in *PT* space. Reactions 2 and 4 are positive. Reaction 3 is slightly negative.

The grid of figure 18 was based on a grid developed by Davidson et al. (1997) for interpreting similar reactions in the Higher Himalayan crystallines

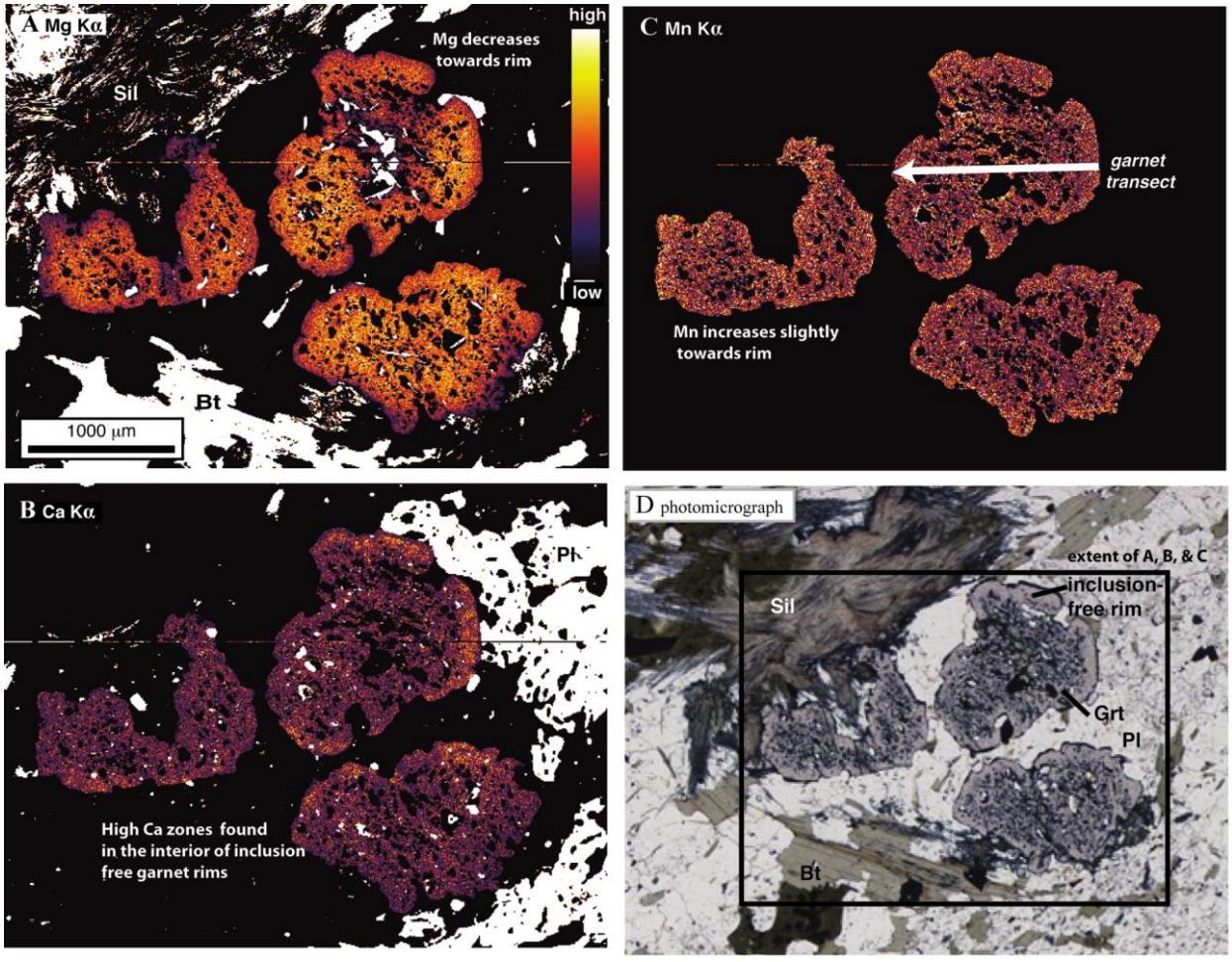

Figure 12. X-ray area scans showing the relative intensity of Mg, Mn, and Ca in the area of TCC-3 shown in figure 4. Arrow in *C* shows the location of the quantitative traverse shown in figure 13. *D* is a photomicrograph of the region of the thin section containing the X-ray scans.

of Bhutan. A version of this grid was introduced by Holdaway et al. (1988). Wei et al. (2004) published a grid topologically similar to that shown in figure 18 but for Mg-free assemblages; that is, it is for an AK(FM) projection. The grid used by Davidson et al. (1997) was constructed for the KFMASH system using the database of Berman (1988; with revisions until 1992). The Davidson grid was constructed for muscovite-present assemblages, whereas that in figure 18 includes muscovite-absent assemblages in order to include the assemblage of sample TCC-3.

The grid shown in figure 18 was calculated for a fixed garnet composition, Alm 74, which approximates the Alm content of garnet of sample KRB-1 and of the garnet used in the grid of Davidson et al. (1997). This grid is for a pseudo three-component, five-phase system, where Fe/Fe + Mg of one of the phases, garnet, is fixed. The chemical system is FeO, Al_2O_3, K_2O with SiO_2, and H_2O in excess. The five phases are muscovite, sillimanite, staurolite, garnet, and biotite (quartz and water in excess). Strictly speaking, the diagram as drawn is for three components. With one added component—for example, Mg—each line becomes a plane in *PT* composition space, and the invariant point, a pseudoinvariant point, becomes a line. Because the garnet composition is Alm 74 along the univariant line for Ms + Grt = Bt + Sil, the biotite composition progressively changes in Mg/Mg + Fe along the line according to the temperature effect on the distribution of Fe and Mg between garnet and biotite. Different garnet compositions would shift the location of the invariant point and reactions 1 and 3 in *PT* space.

The univariant line for St + Q = Grt + Sil (fig. 18) is from the experimental results of the Mg-free system (Richardson 1968); it is applicable for Alm 74 because Mg and Fe fractionation is negligible

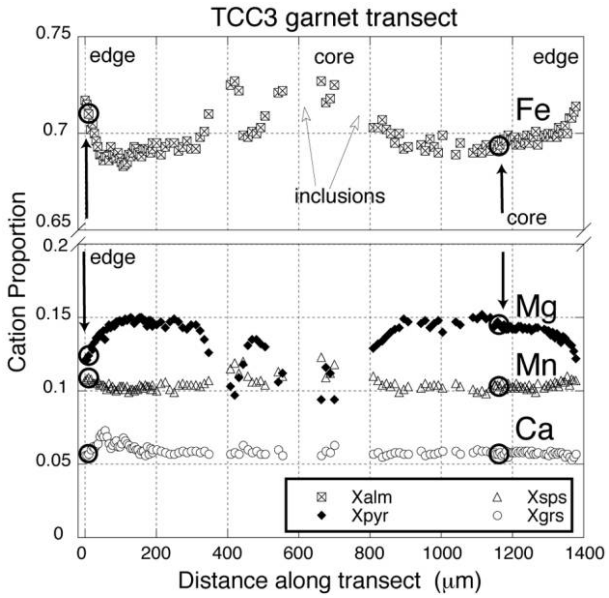

Figure 13. Quantitative traverse across garnet in sample TCC-3 along the transect marked in figure 12*C*. The edge and core compositions are given in table A2 (available in the online edition or from the *Journal of Geology* office).

between staurolite and garnet. However, the location of the reaction is shifted toward lower temperatures with the addition of Mn, which expands the stability field of garnet relative to staurolite.

For sample KRB-1, the location of the pseudoinvariant point is taken to be at 570°C and 4.1 kbar, on the basis of our analysis of a pseudosection for this rock. This reflects a shift of the location of the pseudoinvariant point of Davidson et al. (1997) from 600°C and 4 kbar as a result of the higher Mn of sample KRB-1 compared with the Bhutan samples.

The *PT* path for sample KRB-1 crosses reaction 1 at a temperature above the staurolite breakdown reaction 2. The presence of relict fragments of St in sample KRB-1 implies that reaction 2 was crossed before reaction 1. The path for sample RB-14 crosses reaction 2 at lower temperature and also implies decompression. For the garnet composition of sample TCC-3, the pressure of the invariant point is higher, such that this sample crossed reaction 4 but not reaction 2 at a higher pressure than the pseudoinvariant point shown in figure 18.

All three reactions imply decompression at temperatures close to 600°C, the staurolite-bearing samples below 600°C, and the staurolite-absent rocks above 600°C. There is no record in the southern Tusas Mountains that this temperature was greater than 625°C; the absence of evidence for partial melting is key for constraining the maximum temperature. At 625°C, the presence of early kyanite in quartz veins constrains the maximum pressure to have been above 6 kbar, since the kyanite-sillimanite stability boundary at 625°C is at 6 kbar. The absence of an external heat source in the area, indicated by the lack of exposed 1.4-Ga plutons in the region, and the electron microprobe data described below support the conclusion that the temperatures were at about 600°C during decompression from the kyanite stability field.

***PT* Estimates with TWQ.** We estimated the pressure and temperature conditions for core and rim garnet and plagioclase compositions using TWQ 2.34 (Berman 1991; http://gsc.nrcan.gc.ca/sw/twq_e.php) and the internally consistent thermodynamic database of Berman and Aranovich (1996; updated in 2007; Berman et al. 2007). *PT* estimates were calculated using the intersection of the gar-

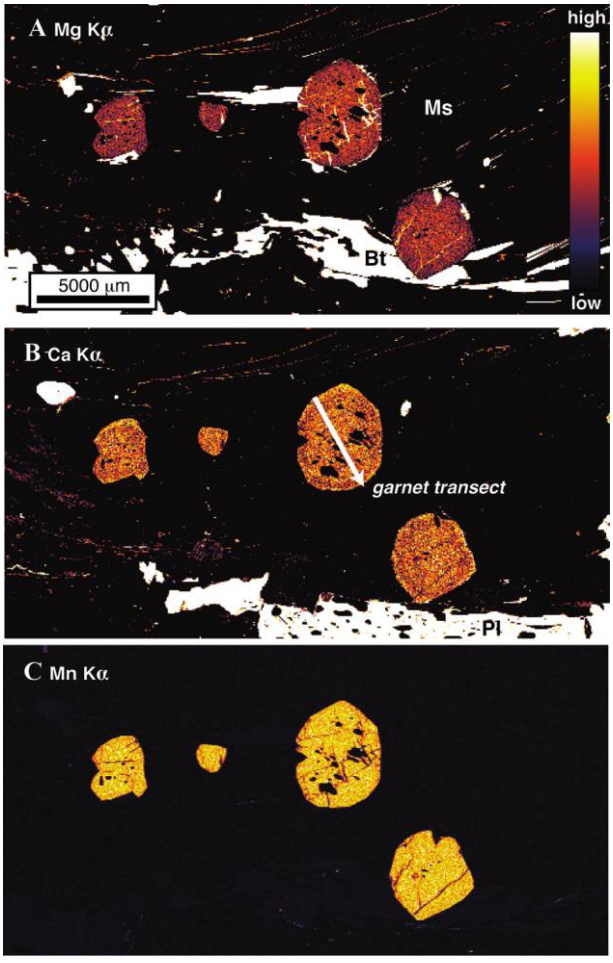

Figure 14. X-ray area scans showing the relative intensity of Mg, Mn, and Ca in the area of PW-2 shown in figure 15. Arrow in *B* shows the location of the quantitative traverse of figure 17.

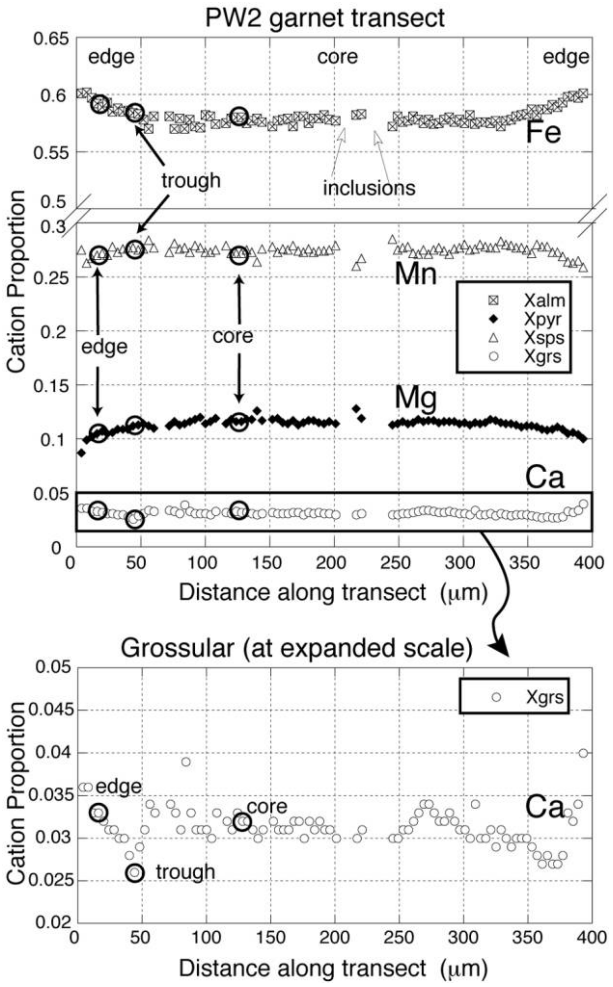

Figure 15. Quantitative traverse across garnet of PW-2 along the transect marked in figure 14*B*. The edge, trough, and core compositions are given in table A2 (available in the online edition or from the *Journal of Geology* office).

net-biotite Fe-Mg exchange thermometer, the GASP barometer, and the eastonite barometer. For all samples, core and rim garnet and plagioclase pairs were used along with the matrix biotite and muscovite composition. For sample PW-2, a "trough" estimate was made using the "trough" garnet composition and the rim plagioclase composition. For sample KRB-1, the composition of the core of the plagioclase included in garnet was used with the core garnet composition, and the matrix plagioclase composition was used with the rim garnet composition.

We found that *PT* estimates did not yield *PT* conditions in the stability fields of the mineral assemblages (fig. 19). With the exception of a TWQ calculation applied to the core of the garnet of sample TCC-3, which gives 4 kbar and 570°C, the results were in the andalusite stability field (2–3 kbar) at temperatures of 500°–550°C. We interpret this to indicate that the garnet compositions no longer record the peak metamorphic conditions.

Pseudosections. We calculated pseudosections for each of the samples. Modes were determined by point counting and by analysis of full-slide X-ray maps. Bulk composition estimates were calculated by integrating modal observations with single mineral analyses (table A7). Pseudosections illustrate what mineral assemblage in what proportions a rock would have over a prescribed portion of *PT* space, given the bulk composition. To calculate pseudosections, we used Theriak-Domino (de Capitani and Petrakakis 2010), which is based on the Gibbs free energy minimization routine algorithm of de Capitani and Brown (1987) with the Holland and Powell (1998) database.

The pseudosection results for sample KRB-1 are consistent with the phase assemblages and the pressures and temperatures inferred from the above petrogenic grid but not those calculated with TWQ (fig. 20). In the pseudosection, contours for the Alm, Sps, and Pyr components in garnet do not correspond to the phase fields for the assemblages; however, those for Grs do correspond to the observed phase field. We used the intersections of calculated isopleths for Grs in garnet and An for plagioclase

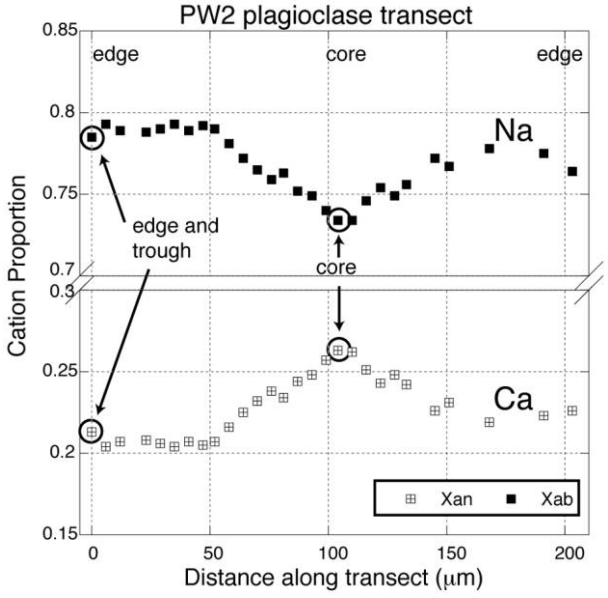

Figure 16. Quantitative traverse across a plagioclase grain in sample PW-2. The edge and core compositions are given in table A3 (available in the online edition or from the *Journal of Geology* office).

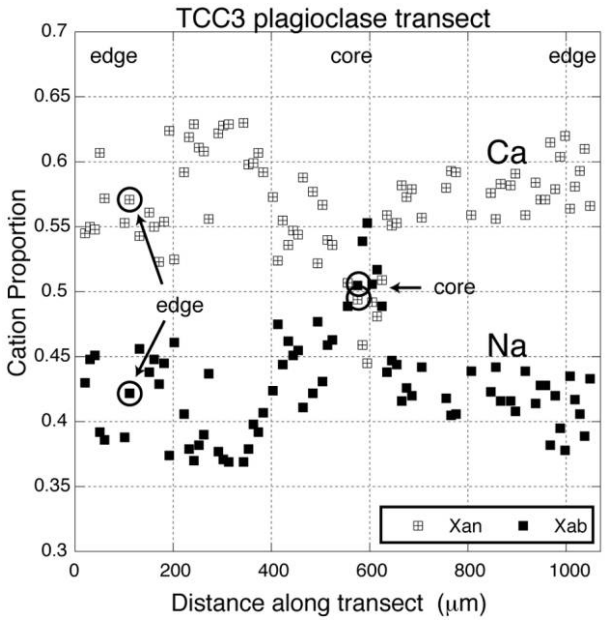

Figure 17. Quantitative traverse across a plagioclase grain in sample TCC-3. The edge and core compositions are given in table A3 (available in the online edition or from the *Journal of Geology* office).

(the inclusion in garnet and the grains in the matrix) on the pseudosection for sample KRB-1 to determine a pressure and temperature of 4 ± 0.3 kbar and 590° ± 10°C. Although we see evidence that growth-related compositional zonation in Fe, Mg, and Mn has been destroyed, we believe that Ca isoleths can be used to help estimate the *P* and *T* at the end of metamorphism. This is a reasonable result, since Ca has a lower diffusivity in garnet than Fe, Mg, and Mn (Carlson 2006). Diffusion of Ca in both garnet and plagioclase essentially does not occur at the temperatures of the Cerro Colorado metamorphism. We interpret this to be the approximate *P* and *T* at the end of the decompression phase of the metamorphism. We acknowledge that a piece of reality that Theriak-Domino cannot account for is the shifting bulk rock composition during garnet growth. Because of the splotchy nature of the Ca in garnet in sample KRB-1 (fig. 10*B*) and the presence of the highly irregular plagioclase inclusion (fig. 10*B*), we do not believe that any mineral compositions preserved in the samples correspond to the earliest conditions of metamorphism.

Discussion

Interpretation of Garnet Zoning. Aside from the zoning across rims, garnets are strikingly homogeneous. They show no record of zoning formed during growth as the garnet depletes the matrix of Mn (Hollister 1966). Rather, the garnets show zoning patterns typical of high-grade garnets that had time to internally homogenize following growth (Woodsworth 1977).

The partially resorbed garnet of sample TCC-3 has a slight increase in Mn at the rims, but this increase does not track with the Fe-Mg zoning. This zoning pattern is typical of back diffusion in garnet in response to resorption during decreasing temperature (Kohn and Spear 2000). The fact that an increase in Mn at the rims is barely detectable in sample TCC-3 and is not present at all in the other samples implies that the garnets do not record a drop in temperature. In fact, Mn decreases toward the rims in samples PW-2 and KRB-1. Thus, the overall picture, based on garnet zoning characteristics, is that the garnets were held at close to peak temperatures (575°–625°C) for long enough that primary compositional zoning in Mg, Fe, and Mn was relaxed by diffusion (Ganguly et al. 1996).

PT estimates made using garnet core compositions in samples KRB-1 and TCC-3 do not record

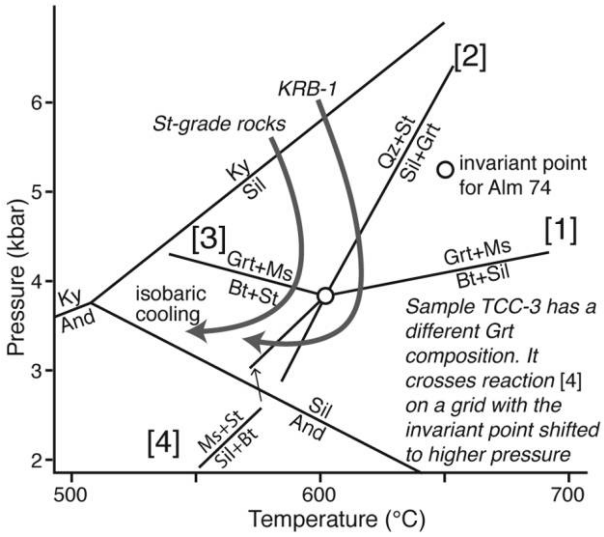

Figure 18. Petrogenetic grid for Fe-Mg units of Cerro Colorado based on a grid developed by Davidson et al. (1997). The grid is calculated for a fixed garnet composition, Alm 74, and is for a pseudo three-component, five-phase system, where Fe/Fe + Mg of one of the phases, garnet, is fixed, and quartz and water are in excess. Arrows show the *PT* paths taken by sample KRB-1 and staurolite grade rocks, such as RB-14, on the basis of observed reaction textures. A path for TCC-3 is not shown because the pressure of the invariant point is higher. All three reactions imply decompression at temperatures close to 600°C, with the staurolite bearing samples below 600°C and the staurolite absent rocks above 600°C.

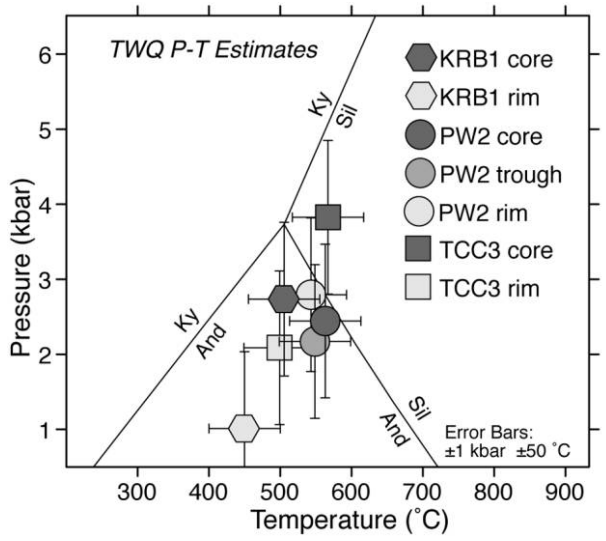

Figure 19. Pressure and temperature conditions for core and rim garnet and plagioclase compositions pairs (tables A2, A3 [available in the online edition or from the *Journal of Geology* office]) calculated using TWQ 2.34 (Berman 1991; http://gsc.nrcan.gc.ca/sw/twq_e.php) and the internally consistent thermodynamic database of Berman and Aranovich (1996; updated in 2007; Berman et al. 2007). With the exception of the core of the garnet of sample TCC-3, *PT* estimates do not yield conditions in the stability fields of the mineral assemblages

peak metamorphic conditions consistent with the stability field of the interpreted peak metamorphic mineral assemblage. Indeed, with the exception of the core garnet in sample TCC-3, the TWQ thermobarometry yielded *PT* conditions outside the stability fields of the observed mineral assemblages (fig. 19). We interpret the inconsistency between *PT* estimates made using the mineral compositions (TWQ; fig. 19) and the bulk rock composition (Theriak-Domino pseudosection; fig. 20) to indicate that there is disequilibrium between the Fe, Mg, and Mn garnet compositions and the rest of the mineral compositions. However, we see evidence that the Ca components of garnet and plagioclase retain reasonable *PT* conditions.

We see evidence for multiple episodes of garnet growth and equilibration. First, the compositionally homogeneous garnets include the earliest foliation recognized in the area. Second, garnet was resorbed in the reaction that formed sillimanite clots. The orientation of the sillimanite clots indicates that sillimanite growth occurred during the main phase of D_2 deformation and before D_3 deformation. Partial reequilibration toward the subsequent lower-pressure conditions occurred during decompression, indicated by the sharp zoning of the rims of the garnet. The drop in pressure thus took place during and after formation of the S_2 foliation. Finally, the late garnets, as described here for sample PW-2, grew after formation of the S_2 foliation.

Proposed* PT *Time Path. Mineral textures show that metamorphism of the rocks of Cerro Colorado began at conditions where kyanite and garnet were stable. The early garnet remained at high enough *T* and for long enough that its composition was homogenized. There is no record in the southern Tusas Mountains that this *T* was greater than 625°C. Accordingly, garnet (and staurolite) must have resided at 600°–625°C for a substantial period of time. At 625°C, the presence of kyanite constrains the maximum *P* to have been 6 kbar or more (fig. 18). The unzoned garnet and absence of lower-grade minerals such as chloritoid cannot be reconciled with models of near isobaric heating by an external source to reach the *P*′s and *T*′s recorded in the Cerro Colorado rocks.

New reactions were initiated by a drop in pressure at close to peak metamorphic temperatures. Kyanite was partially to completely replaced by sil-

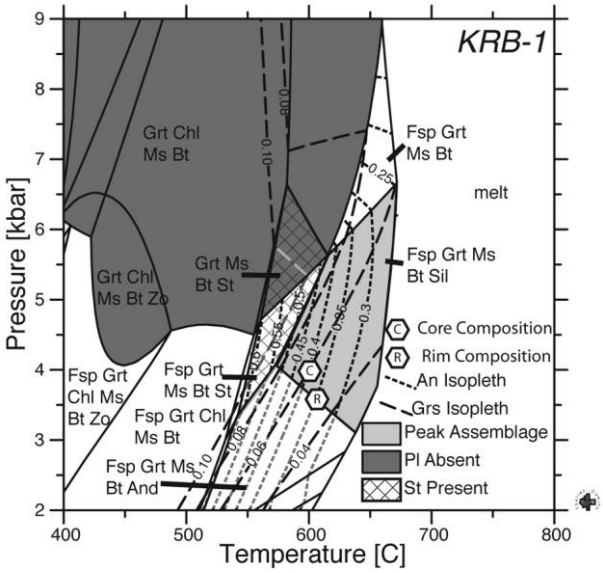

Figure 20. Pseudosection for sample KRB-1. Modes were determined by point counting and by analysis of full-slide X-ray maps. Pseudosection calculated by Theriak-Domino (de Capitani and Brown 1987; de Capitani and Petrakakis 2010) with the Holland and Powell (1998) database. The results are consistent with the phase assemblages and the pressures and temperatures inferred from the petrogenic grid but not those calculated with TWQ. Contours for the Alm, Sps, and Pyr components in garnet do not correspond to the phase fields for the assemblages; however, those for Grs do correspond to the correct phase field.

limanite. As pressure dropped, the rocks crossed two reaction curves that have shallow slopes in *PT* space, one at a lower temperature than the other. These reactions consumed garnet and produced staurolite (RB-14) and sillimanite (KRB-1). The composition of any remaining garnet was modified as a result of these reactions. The pressure was about 4 kbar at the end of the decompression. This pressure is constrained by the rocks being in the sillimanite stability field but above that of the pseudoinvariant point of figure 18. This is confirmed by the location of the Grs and An isopleths on the pseudosection of sample KRB-1.

The time of decompression is interpreted to be between 1.4 and 1.47 Ga on the basis of the relationship between the observed decompression reaction, microstructure development, and reported constraints on the timing of the microstructure development. Our petrologic observations indicate that the decompression and associated sillimanite growth occurred during and after formation of the S_2 foliation. The younger limit on the timing of S_2 is given by coarse pegmatites that crosscut S_2 and yield U-Pb monazite dates and concordant U-Pb titanite and xenotime dates of 1.41–1.42 Ga (Williams et al. 1999*a*).

The constraints for the older limit on the timing of S_2 are more elusive. The best constraint for the timing of S_2 comes from monazite from Cerro Colorado, described by Williams et al. (1999*b*). This monazite is included within porphyroblasts of staurolite and is aligned with the regional foliation. At Cerro Colorado, we observe that the regional foliation is S_2. The monazite is zoned but has only one age domain that yields microprobe dates of 1.4–1.45 Ga (Williams et al. 1999*b*). We interpret the alignment of the monazite to indicate that S_2 developed at 1.4–1.45 Ga.

The dates reported for monazite in the staurolite schist and in the syn-D_3 pegmatites support the conclusion that S_2 developed at 1.4–1.45 Ga (reported in Bishop 1997; Williams et al. 1999*a*, 1999*b*). This indicates that the decompression reaction that produced sillimanite aligned in S_2 and folded by F_3 folds occurred at 1.4–1.45 Ga. After decompressing, the rocks cooled isobarically between 1.4 and 1.3 Ga, as reported for throughout northern New Mexico on the basis of Ar cooling dates (Shaw et al. 2005). Williams et al. (1999*a*) interpret the monazite inclusions in staurolite to represent the timing of M_3 and suggest that M_2 and D_2 could be at either ca. 1.4 or 1.65 Ga.

Ductile Thrusting. The schists with the abundant sillimanite clots are structurally about 300 m above the garnet-staurolite schists (fig. 2) when measured in a section parallel to the L_2 lineations. The section starts at the staurolite sample locale (RB-14) in figure 2, with S_2 foliations that dip 35° north, and extends north 0.5 km horizontally to the sillimanite clot schists, which also dip 35° north. The sillimanite clot schists are the same unit from which sample KRB-1 was collected but are on the flank rather than the nose of the F_3 antiform.

The observation that before F_3 folding, the higher-temperature sillimanite schists (e.g., KRB-1) are structurally above the lower-temperature staurolite schists (e.g., TCC-3 and RB-14) implies an inverted metamorphic sequence. Because there are no observed heat sources (e.g., plutons) structurally above the sillimanite schists, the temperature inversion implies the hot on cold relation was established by thrusting.

The inverted metamorphic sequence can be interpreted in the context of the down-plunge projection of the Tusas Mountains given in figure 3 of Williams (1991) and revised as figure 2 of Williams et al. (1999*a*). The section has been thickened by recumbent folds and nappes thrust from south to north above a decollement between the metasedimentary layers and the underlying 1.65-Ga Tres Piedras granite. The Cerro Colorado antiform appears in the sections as an out-of-sequence antiformal uplift rooted near the decollement, which projects to some 10 km below the present level of exposure at Cerro Colorado.

We found no evidence at the present level of exposure in the Cerro Colorado area that melt was present during the thrusting. However, the pegmatites that intruded after D_3 (Williams et al. 1999*a*) suggest that melt was present at structurally deeper levels. The age of these pegmatites is 1.41–1.42 Ga (reported in Williams et al. 1999*a*) and corresponds to ages of plutons elsewhere in northern New Mexico. Our interpretation of the metamorphic history of the Cerro Colorado area can therefore include granitic melts at deeper levels.

Implications for Tectonic History of Northern New Mexico. Our results define a clockwise *PT* loop (fig. 18). The phase of decompression of the loop appears to have been concurrent with the 1.40–1.45-Ga thermal event of northern New Mexico. This is based on correlating the decompression reactions involving Fe-Mg silicates with the dates attributed to growth of the metamorphic minerals. Having the decompression phase of the loop at 1.4 Ga is counter to the prevailing interpretation that the decompression occurred at 1.6–1.7 Ga (Williams and Karlstrom 1996; Wiliams et al. 1999*a*; Karlstrom et al. 2004). Other studies have noted the presence of early kyanite but begin a clockwise

PT loop from the kyanite field, back to a normal geothermal gradient, and then reheating with hairpin turns at metamorphic conditions achieved near 1.4 Ga (Williams and Karlstrom 1996). This *PT* path for northern New Mexico requires heating as pressure drops at 1.6–1.7 Ga. For the 1.4-Ga decompression interpretation of this article, no added heat is necessary to produce the observed reactions and assemblages. The decompression can begin from points on the geothermal gradient within the field of stability of kyanite. The heat was present from the start of the decompression, at above 6 kbar. The clockwise *PT* loop at 1.4 Ga for the Cerro Colorado area is consistent with that proposed for the Picuris (fig. 1) by Daniel and Pyle (2006), which was based on reaction textures among the aluminum silicates. Daniel and Pyle (2006) argued for a 1-kbar decrease in pressure while at peak temperature. Our observations are also consistent with the alternate tectonic model proposed by Pedrick et al. (1998; fig. 12*B*) for the Taos Range of northern New Mexico. This model considers that all the metamorphism in northern New Mexico was at ca. 1.4 Ga and argues for 3–5 kbar of decompression. The main difference between the interpretation of our results and those of Daniel and Pyle (2006) and the alternate model of Pedrick et al. (1998) is the amount of decompression we propose.

Conclusions

We describe decompression reactions from the Cerro Colorado area, southern Tusas Mountains, New Mexico. The magnitude of decompression is approximately 2 kbar, from 6 to 4 kbar, and it occurred at temperatures of 575°–625°C. Published chronologic data imply that the decompression occurred at 1.4–1.45 Ga. These observations are contrary to previous interpretations for the Cerro Colorado area (Williams and Karlstrom 1996) that call for an episode of isobaric heating in this time interval.

The metamorphic zones are locally inverted, with higher-temperature rocks structurally above lower-temperature rocks. This inversion was likely a consequence of the top to north ductile thrusting mapped in the Tusas Mountains (Williams 1991). The decompression would be a result of tectonic and/or erosional denudation in response to crustal thickening due to the ductile thrusting.

Key observations are the nearly homogeneous garnet relicts and early kyanite, which indicate that the rocks were at moderate temperature and pressure for a long period of time before the decompression. The decompression is recorded best by the reaction Grt + Ms = Sil + Bt.

ACKNOWLEDGMENTS

We thank M. Williams and M. Jercinovic for assistance in the collection of the microprobe data. We also thank R. Martin and M. Martin for their hospitality while we were working in New Mexico, and we thank all past undergraduate petrology students at Princeton University for providing the basis for this study, in particular, J. Chadwick, D. T. Cecil-Cockwell, and R. Bernard. J. Chadwick also provided immeasurable help in preparing the figures and in collecting the sample and providing the photo of figure 9. K. R. Barnhart thanks A. Ault and K. Mahan for discussion and help with microstructural interpretation and G. Dumond for discussion and help while collecting microprobe data. Constructive and thorough reviews by E. Duebendorfer and M. "Pat" Bickford greatly improved the quality and clarity of the manuscript. This research was funded by National Science Foundation awards EAR-0310223 to L. S. Hollister and EAR-1019817 to C. L. Andronicos.

REFERENCES CITED

Amato, J. M.; Heizler, M. T.; Boullion, A. O.; Sanders, A. E.; Toro, J.; McLemore, V. T.; and Andronicos, C. L. 2011. Syntectonic 1.46 Ga magmatism and rapid cooling of a gneiss dome in the southern Mazatzal Province: Burro Mountains, New Mexico. Geol. Soc. Am. Bull. 123:1720–1744.

Anderson, J. L. 1983. Proterozoic anorogenic granite plutonism in North America. Geol. Soc. Am. Mem. 161: 133–154.

Barnhart, K. R. 2008. Metamorphism of Proterozoic rocks in north central New Mexico based on quantitative thermobarometry. BSE thesis, Princeton University, Princeton, NJ.

Berman, R. 1988. Internally-consistent thermodynamic data for minerals in the system Na_2O-K_2O-CaO-MgO-FeO-Fe_2O_3-Al_2O_3-SiO_2-TiO_2-H_2O-CO_2. J. Petrol. 29: 445–522.

Berman, R.; Aranovich, L.; Rancourt, D.; and Mercier, P. H. J. 2007. Reversed phase equilibrium constraints on the stability of Mg-Fe-Al biotite. Am. Mineral. 92: 139–150.

Berman, R. G. 1991. Thermobarometry using multi-equi-

librium calculations: a new technique, with petrological applications. Can. Mineral. 29:833–855.

Berman, R. G., and Aranovich, L. Y. 1996. Optimized standard state and solution properties of minerals. Contrib. Mineral. Petrol. 126:1–24.

Bickford, M. E., and Hill, B. M. 2007. Does the arc accretion model adequately explain the Paleoproterozoic evolution of southern Laurentia? an expanded interpretation. Geology 35:167.

Bishop, J. 1997. The determination of a quantitative P-T-t-D history for Proterozoic rocks of the Cerro Colorado area, north central New Mexico. MS thesis, University of Massachusetts, Amherst.

Bowring, S. A., and Karlstrom, K. E. 1990. Growth, stabilization, and reactivation of Proterozoic lithosphere in the southwestern United States. Geology 18:1203–1206.

Carlson, W. D. 2006. Rates of Fe, Mg, Mn, and Ca diffusion in garnet. Am. Mineral. 91:1–11.

Cather, S. M.; Karlstrom, K. E.; Timmons, J. M.; and Heizler, M. T. 2006. Palinspastic reconstruction of Proterozoic basement-related aeromagnetic features in north-central New Mexico: implications for Mesoproterozoic to late Cenozoic tectonism. Geosphere 2:299.

Cavosie, A., and Selverstone, J. 2003. Early Proterozoic oceanic crust in the northern Colorado Front Range: implications for crustal growth and initiation of basement faults. Tectonics 22:1015, doi:10.1029/2001TC001325.

Daniel, C., and Pyle, J. 2006. Monazite-xenotime thermochronometry and Al_2SiO_5 reaction textures in the Picuris range, northern New Mexico, USA: new evidence for a 1450–1400 Ma orogenic event. J. Petrol. 47:97–118.

Davidson, C.; Grujic, D. E.; Hollister, L. S.; and Schmid, S. M. 1997. Metamorphic reactions related to decompression and synkinematic intrusion of leucogranite, High Himalayan crystallines, Bhutan. J. Metamorph. Geol. 15:593–612.

de Capitani, C., and Brown, T. 1987. The computation of chemical equilibrium in complex systems containing non-ideal solutions. Geochim. Cosmochim. Acta 51(suppl.):2639–2652.

de Capitani, C., and Petrakakis, K. 2010. The computation of equilibrium assemblage diagrams with Theriak/Domino software. Am. Mineral. 95:1006–1016.

Ferguson, C. B.; Duebendorfer, E. M.; and Chamberlain, K. R. 2004. Synkinematic intrusion of the 1.4-Ga Boriana Canyon pluton, northwestern Arizona: implications for ca. 1.4-Ga regional strain in the western United States. J. Geol. 112:165–183.

Ganguly, J.; Chakraborty, S.; Sharp, T. G.; and Rumble, D. 1996. Constraint on the time scale of biotite-grade metamorphism during Acadian orogeny from a natural garnet-garnet diffusion couple. Am. Mineral. 81:1208–1216.

Grambling, J. 1981. Kyanite, andalusite, sillimanite, and related mineral assemblages in the Truchas Peaks region, New Mexico. Am. Mineral. 66:702–722.

———. 1988. A summary of Proterozoic metamorphism in northern New Mexico: the regional development of 520°C, 4 kbar rocks. *In* Ernst, W. G., ed. Metamorphism and crustal evolution of the western United States. Englewood Cliffs, NJ, Prentice Hall, p. 446–465.

Grambling, J. A., and Dallmeyer, R. D. 1993. Tectonic evolution of Proterozoic rocks in the Cimarron Mountains, northern New Mexico, USA. J. Metamorph. Geol. 11:739–755.

Grambling, J. A.; Williams, M. L.; Smith, R. F.; and Mawer, C. K. 1989. The role of crustal extension in the metamorphism of Proterozoic rocks in northern New Mexico. Geol. Soc. Am. Spec. Pap. 235:87–110.

Hill, B., and Bickford, M. E. 2001. Paleoproterozoic rocks of central Colorado: accreted arcs or extended older crust? Geology 29:1015–1018.

Holdaway, M. J. 1978. Significance of chloritoid-bearing and staurolite-bearing rocks in the Picuris Range, New Mexico. Geol. Soc. Am. Bull. 89:1404–1414.

Holdaway, M. J.; Durnow, B.; and Hinton, R. W. 1988. Devonian and Carboniferous metamorphism in west-central Maine: the muscovite-almandine geobarometer and the staurolite problem revisited. Am. Mineral. 73:20–47.

Holland, T., and Powell, R. 1998. An internally consistent thermodynamic data set for phases of petrological interest. J. Metamorph. Geol. 16:309–334.

Hollister, L. S. 1966. Garnet zoning: an interpretation based on the Rayleigh fractionation model. Science 154:1647–1651.

Jones, J. V., III; Daniel, C. G.; Frei, D.; and Thrane, K. 2011. Revised regional correlations and tectonic implications of Paleoproterozoic and Mesoproterozoic metasedimentary rocks in northern New Mexico, USA: new findings from detrital zircon studies of the Hondo Group, Vadito Group, and Marqueñas Formation. Geosphere 7:974.

Karlstrom, K., and Daniel, C. G. 1993. Restoration of Laramide right-lateral strike slip in northern New Mexico by using Proterozoic piercing points: tectonic implications from the Proterozoic to the Cenozoic. Geology 21:1139–1142.

Karlstrom, K., and Houston, R. 1984. The Cheyenne belt: analysis of a Proterozoic suture in southern Wyoming. Precambrian Res. 25:415–446.

Karlstrom, K. E.; Amato, J. M.; Williams, M. L.; Heizler, M. T.; Shaw, C. M.; Read, A. S.; and Bauer, P. W. 2004. Proterozoic tectonic evolution of the New Mexico region: a synthesis. *In* Mack, G. H., and Guiles, K. A., eds. The geology of New Mexico. N. M. Geol. Soc. Spec. Publ. 11:1–35.

Karlstrom, K. E., and Bowring, S. A. 1988. Early Proterozoic assembly of tectonostratigraphic terranes in southwestern North America. J. Geol. 96:561–576.

Karlstrom, K. E.; Dallmeyer, R. D.; and Grambling, J. A.

1997. $^{40}Ar/^{39}Ar$ evidence for 1.4 Ga regional metamorphism in New Mexico: implications for thermal evolution of lithosphere in the southwestern USA. J. Geol. 105:205–224.

Kirby, E.; Karlstrom, K. E.; Andronicos, C. L.; and Dallmeyer, R. D. 1995. Tectonic setting of the Sandia pluton: an orogenic 1.4 Ga granite in New Mexico. Tectonics 14:185–201.

Kohn, M. J., and Spear, F. 2000. Retrograde net transfer reaction insurance for pressure-temperature estimates. Geology 28:1127–1130.

Koning, D.; Karlstrom, K. E.; May, J.; Skotnicki, S. J.; Horning, R.; Newell, D.; and Muehlberger, W. R. 2005. Preliminary geologic map of the Ojo Caliente 7.5-minute quadrangle, Rio Arriba and Taos Counties, New Mexico. Open-File Geologic Map. Socorro, NM, New Mexico Bureau of Geology and Mineral Resources.

Lanzirotti, A.; Bishop, J.; and Williams, M. 1996. A more vigorous approach to dating mid-crustal processes: U-Pb dating of varied major and accessory metamorphic minerals tied to microstructural studies. Geol. Soc. Am. Abstr. Prog., p. 453.

Nyman, M. W.; Karlstrom, K. E.; Kirby, E.; and Graubard, C. M. 1994. 1.4 Ga contractional orogeny in western North America: evidence from ca. 1.4 Ga plutons. Geology 22:901–904.

Pedrick, J. N.; Karlstrom, K. E.; and Bowring, S. A. 1998. Reconciliation of conflicting tectonic models for Proterozoic rocks of northern New Mexico. J. Metamorph. Geol. 16:687–707.

Richardson, S. 1968. Staurolite stability in a part of the system Fe-Al-Si-O-H. J. Petrol. 9:467–488.

Shaw, C.; Heizler, M.; and Karlstrom, K. 2005. $^{40}Ar/^{39}Ar$ thermochronologic record of 1.45–1.35 Ga intracontinental tectonism in the southern Rocky Mountains: interplay of conductive and advective heating with intracontinental deformation. Geophys. Monogr. 154: 163–184.

Shaw, C., and Karlstrom, K. E. 1999. The Yavapai-Mazatzal crustal boundary in the southern Rocky Mountains. Rocky Mt. Geol. 34:37–52.

Treiman, A. H. 1977. Precambrian geology of the Ojo Caliente quadrangle, Rio Arriba and Taos Counties, New Mexico. Stanford, CA, Stanford University Press.

Tyson, A.; Morozova, E.; Karlstrom, K.; Chamberlain, K. R.; Smithson, S. B.; Dueker, K. G.; and Foster, C. T. 2002. Proterozoic Farwell Mountain–Lester Mountain suture zone, northern Colorado: subduction flip and progressive assembly of arcs. Geology 30:943–946.

Wei, C.; Powell, R.; and Clarke, G. L. 2004. Calculated phase equilibria for low- and medium-pressure metapelites in the KFMASH and KMnFMASH systems. J. Metamorph. Geol. 22:495–508.

Whitney, D. L., and Evans, B. W. 2010. Abbreviations for names of rock-forming minerals. Am. Mineral. 95: 185–187.

Williams, M.; Jercinovic, M.; and Terry, M. P. 1999*a*. Age mapping and dating of monazite on the electron microprobe: deconvoluting multistage tectonic histories. Geology 27:1023–1026.

Williams, M.; Karlstrom, K.; Lanzirotti, A.; Read, A.; Bishop, J.; Lombardi, C.; Pedrick, J.; and Wingsted, M. 1999*b*. New Mexico middle-crustal cross sections: 1.65-Ga macroscopic geometry, 1.4-Ga thermal structure, and continued problems in understanding crustal evolution. Rocky Mt. Geol. 34:53.

Williams, M. L. 1991. Heterogeneous deformation in a ductile fold-thrust belt: the Proterozoic structural history of the Tusas Mountains, New Mexico. Geol. Soc. Am. Bull. 103:171–188.

Williams, M. L., and Karlstrom, K. E. 1996. Looping *PT* paths and high-*T*, low-*P* middle crustal metamorphism: Proterozoic evolution of the southwestern United States. Geology 24:1119–1122.

Woodsworth, G. J. 1977. Homogenization of zoned garnets from pelitic schists. Can. Mineral. 15:230–242.